ELSEVIER

Integrated surface–groundwater flow modeling: A free-surface overland flow boundary condition in a parallel groundwater flow model

Stefan J. Kollet *, Reed M. Maxwell

*Atmospheric, Earth, and Energy Sciences Department, Lawrence Livermore National Laboratory (L-206),
7000 East Avenue, Livermore, CA 94550, USA*

Abstract

Interactions between surface and groundwater are a key component of the hydrologic budget on the watershed scale. Models that honor these interactions are commonly based on the conductance concept that presumes a distinct interface at the land surface, separating the surface from the subsurface domain. These types of models link the subsurface and surface domains via an exchange flux that depends upon the magnitude and direction of the hydraulic gradient across the interface and a proportionality constant (a measure of the hydraulic connectivity). Because experimental evidence of such a distinct interface is often lacking in field systems, there is a need for a more general coupled modeling approach.

A more general coupled model is presented that incorporates a new two-dimensional overland flow simulator into the parallel three-dimensional variably saturated subsurface flow code ParFlow [Ashby SF, Falgout RD. A parallel multigrid preconditioned conjugate gradient algorithm for groundwater flow simulations. Nucl Sci Eng 1996;124(1):145–59; Jones JE, Woodward CS. Newton–Krylov-multigrid solvers for large-scale, highly heterogeneous, variably saturated flow problems. Adv Water Resour 2001;24:763–774]. This new overland flow simulator takes the form of an upper boundary condition and is, thus, fully integrated without relying on the conductance concept. Another important advantage of this approach is the efficient parallelism incorporated into ParFlow, which is exploited by the overland flow simulator.

Several verification and simulation examples are presented that focus on the two main processes of runoff production: excess infiltration and saturation. The model is shown to reproduce an analytical solution for overland flow, replicates a laboratory experiment for surface–subsurface flow and compares favorably to other commonly used hydrologic models. The influence of heterogeneity of the shallow subsurface on overland flow is also examined. The results show the propagation of uncertainty due to subsurface heterogeneity to the overland flow predictions and demonstrate the usefulness of our approach. Both the overland flow component and the coupled model are evaluated in a parallel scaling study and show to be efficient.
© 2005 Elsevier Ltd. All rights reserved.

Keywords: Surface-groundwater interactions; Overland flow boundary condition; Integrated parallel modeling; Subsurface heterogeneity; Hydrograph uncertainty

1. Introduction

The subsurface and surface are complex environmental systems that often behave in a coupled manner. Surface water in rivers, streams, lakes and wetlands is in constant communication with the vadose zone, shallow

* Corresponding author. Tel.: +1 925 422 9297; fax: +1 925 422 3118.
  E-mail address: kollet2@llnl.gov (S.J. Kollet).

and deep groundwater systems. Thus, surface–groundwater interactions are an intrinsic component of the hydrologic budget on the watershed scale and hydrologic modeling tools must account for this interaction to provide reliable predictions. Surface–groundwater interactions have been a widely recognized research area by several scientific communities interested in different spatial scales varying from bedform scale in hyporheic exchange modeling to continental scale hydrologic response modeling.

The occurrence of surface water and its spatial and temporal distribution depends on climatic factors (e.g., amount and distribution of rainfall and temperature), vegetation, topography (micro and macro), and on the exchange of water between the surface and the subsurface. The rate and direction of exchange (groundwater discharge at the land surface or surface water infiltration into the subsurface) depend on the rainfall rate, direction of the hydraulic gradient and hydraulic characteristics of the land surface.

The two major processes of runoff production are commonly referred to as Hortonian and Dunne runoff. Hortonian runoff, often referred to as excess infiltration, occurs when the rainfall rate exceeds the saturated hydraulic conductivity of the land surface. Under excess infiltration conditions, ponding (accumulation of water at the surface) can occur before the subsurface becomes entirely saturated [26]. Dunne runoff, often referred to as excess saturation, occurs when the rainfall rate is smaller or equal to the saturated hydraulic conductivity of the land surface. Under excess saturation conditions, ponding can occur only when the entire soil column becomes completely saturated and water exfiltrates at the surface [26]. Although these two processes are often considered independent, in the presence of a nonuniform distribution of soil properties, infiltration and saturation excess are interrelated and may occur simultaneously at various spatial and temporal scales.

Traditionally, the coupling of the surface and subsurface domains has been done via an exchange flux that appears in both the groundwater and surface water flow equations as general sink/source terms. In this approach, the exchange rate is often expressed in terms of the conductance concept, which assumes an interface connecting the two domains (e.g., [2,44]). This interface is commonly characterized by a proportionality constant representing the connectivity between the surface and subsurface and generally involves the ratio of the interface hydraulic conductivity and effective thickness (e.g., [18]). Recent studies have included additional processes into the conductance concept to account for the influence of microtopography on surface saturation [44,32]. The application of the conductance concept to natural systems can be problematic, as some recent field work has shown the absence of a distinct interface between the surface and subsurface [25,7]. Therefore, the proportionality constant often is used as a lumped fitting parameter (e.g. [4,15]). These studies point to the need for an alternate, more general approach to couple surface and subsurface systems that does not rely on an exchange flux term.

Numerical algorithms for solving the problem of variably saturated groundwater flow are widely available and have been published extensively (e.g., [19,24, 12,38,29,22]). Overland flow simulators have been also studied extensively [37,14,11,21]. The coupling of surface and subsurface flow also received considerable attention recently (e.g., the review by [27]), with many models coupled in a linked fashion, iterating over the exchange flux until some convergence criterion is reached. Previous studies are summarized briefly below.

Freeze and Harlan [13] provided the first comprehensive conceptual and theoretical framework of an integrated hydrologic response model on the watershed scale. Later, Govindaraju and Kavvas [16] developed a coupled model that accounts for 1D channel and overland flow and 3D variably saturated groundwater flow. They studied the response of variable source areas (saturated areas adjacent to the stream) to hydrologic and topographic variations. Woolhiser et al. [47] studied the effect of subsurface heterogeneity in the hydraulic conductivity using an overland flow model coupled to the Smith–Parlange infiltration model. They demonstrated the effect of heterogeneity on the hydrograph and presented a technique that accounted for the influence of microtopography. Wallach et al. [45] studied the error in the exchange rate between the surface and the subsurface when the exchange rate is calculated assuming zero ponding depth. Fiedler and Ramirez [11] solved the 2D hydrodynamic flow equations using a MacCormack finite difference method. In their model, interactive infiltration is simulated using the Green–Ampt formulation. Gunduz and Aral [17] solved the problem of coupled groundwater and 1D channel flow simultaneously, by solving the equations in a single matrix instead of two separate matrices, one for each domain. Braunschweig et al. [6] presented an integrated hydrologic modeling system that incorporates routing of water inside channels and over the land surface coupled to infiltration processes. Putti and Paniconi [34] discussed numerical issues, such as the influence of the time step size on the global convergence behavior, in coupling a three-dimensional, variably saturated flow model with a 1D diffusion formulation for the overland flow equations. VanderKwaak and Loague [44] and Panday and Huyakorn [32] presented fully coupled approaches including land surface processes, such as evaporation, and demonstrated their usefulness. A common theme among much of the previous work summarized here is that these models rely on some form of exchange flux and use the conductance concept. The current work presented in this paper differs

from these studies in that it provides a framework for a more general approach.

This study presents a general framework for coupling the surface and groundwater flow equations, which does not rely on the conductance concept. The surface water equations are used to close the initial value problem of variably saturated groundwater flow, which results in an overland flow boundary condition. This overland flow boundary condition, which has not been published before in the presented form to our knowledge, takes into account the free surface of water ponded at the land surface. To demonstrate the usefulness of this approach, a two-dimensional distributed overland flow simulator has been implemented into the three-dimensional, variably saturated groundwater flow code ParFlow [3,22,40]. We present verification and simulation examples that focus on the surface water component independently and the aforementioned processes of excess infiltration and saturation. We introduce subsurface heterogeneity in the hydraulic conductivity tensor resulting in variable surface runoff and hydrograph uncertainty. ParFlow was designed for parallel computer systems and has been used extensively in large-scale and high resolution modeling [3,22]. The overland flow simulator exploits ParFlow's parallel infrastructure effectively and is also fully parallel, which is demonstrated in a parallel efficiency study.

2. Theory

As mentioned in Section 1, the theory of coupled surface water–groundwater systems has been the subject of many previous studies. Hence, the governing equations of overland flow and variably saturated groundwater flow have been discussed in great detail in the literature. We therefore, provide only a brief summary of these equations that form the basis for the set of coupled equations presented later in Section 2.4.

2.1. Shallow overland flow

In two spatial dimensions, the continuity equation can be written as

$$\frac{\partial \psi_s}{\partial t} = \nabla \cdot \vec{v} \, \psi_s + q_r(x) + q_e(x), \tag{1}$$

where t is time [T], $\vec{v}$ is the depth averaged velocity vector [L T^{-1}]; ψ_s is the surface ponding depth [L], $q_r(x)$ is the rainfall rate [L T^{-1}] and $q_e(x)$ is the exchange rate with the subsurface [L T^{-1}], which will be discussed in detail below. Note, that in Eq. (1) the flow depth is vertically averaged. Thus, vertical change of momentum in the column of ponded water is neglected in this formulation. This has been shown to be a good approximation for shallow systems.

If diffusion terms are neglected the momentum equation can be written as

$$S_{f,i} = S_{o,i}, \tag{2}$$

which is commonly referred to as the kinematic wave approximation [8]. In Eq. (2), $S_{o,i}$ is the bed slope (gravity forcing term) [–], which is equal to the friction slope $S_{f,i}$ [–]; i stands for the x- and y-direction. Although, we consider the kinematic wave in the current work, this formulation can be expanded to incorporate the diffusive and dynamic wave equations [11].

Manning's equation (in [8]) is used to establish a flow depth–discharge relationship

$$v_x = \frac{\sqrt{S_{f,x}}}{n} \psi_s^{2/3} \quad \text{and} \quad v_y = \frac{\sqrt{S_{f,y}}}{n} \psi_s^{2/3}, \tag{3}$$

where n [T L$^{-1/3}$] is the Manning's coefficient. This empirical relationship has been widely applied to describe surface water systems. Anisotropy in the Manning's coefficient is not considered here, though it could easily be incorporated.

Water can leave the overland flow domain horizontally only at an outlet. Considering a real system, the outlet can be interpreted as the mouth of a river. At the outlet, two types of boundary conditions were implemented into the overland flow simulator: the gradient and critical depth outlet conditions (Eqs. (4) and (5), respectively)

$$q_{out} = \frac{\sqrt{S_{f,outlet}}}{n_{outlet}} \psi_{s,outlet}^{5/3}, \tag{4}$$

$$q_{out} = \sqrt{g \psi_{s,outlet}^3}, \tag{5}$$

where g is the acceleration due to gravity [L/T^{-2}]. The gradient outlet condition is equivalent to the zero depth gradient condition of Panday and Huyakorn [32] for the diffusive wave equation. The critical depth boundary condition results in a constant flow depth at the outlet.

2.2. Variably saturated groundwater flow

The equation for variably saturated groundwater flow is the well-known Richards' equation [35]

$$S_s S_w \frac{\partial \psi_p}{\partial t} + \phi \frac{\partial S_w(\psi_p)}{\partial t} = \nabla \cdot q + q_s + \frac{q_e}{m'},$$
$$q = -k(x) k_r(\psi_p) \nabla(\psi_p - z), \tag{6}$$

where ψ_p is the subsurface pressure head [L], z is depth below the surface [L], $k(x)$ is the saturated hydraulic conductivity [L T^{-1}], k_r is the relative permeability [–] (a function of pressure head, ψ_p), S_s is the specific storage coefficient [L^{-1}], ϕ is the porosity [–], S_w is the degree-of-saturation [–], q_s is the general source/sink term [T^{-1}], q_e is the exchange rate with the surface [L T^{-1}] and m' is the thickness of an interface separating the surface and subsurface domains [L]. The datum is

located at the ground surface ($z = 0$) with the negative z-axis pointing downward. In the current formulation, the vanGenuchten [42] relationships are used to describe the relative saturation and permeability functions.

$$S_w(\psi_p) = \frac{s_{sat} - s_{res}}{(1 + (\alpha\psi_p)^n)^{(1-1/n)}} + s_{res}, \quad (7)$$

$$kr(\psi_p) = \frac{\left(1 - \frac{(\alpha\psi_p)^{n-1}}{(1+(\alpha\psi_p)^n)^{(1-1/n)}}\right)^2}{(1 + (\alpha\psi_p)^n)^{\frac{(1-1/n)}{2}}}, \quad (8)$$

where α [L^{-1}] and n [–] are soil parameters, s_{sat} [–] is the relative saturated water content and s_{res} [–] is the relative residual saturation.

The boundary conditions are of the Neumann type

$$-k(x)k_r\nabla(\psi_p - z) = q_{bc}, \quad (9)$$

on Γ, but can be changed to the Dirichlet type if necessary.

2.3. Exchange flux

In previous efforts (e.g., [43,32]), an exchange flux q_e was used to couple the surface and the subsurface domains. It generally follows the form

$$q_e(x) = \lambda(x)(\psi_s - \psi_p). \quad (10)$$

Thus, the exchange rate depends upon the gradient across some interface and the proportionality constant $\lambda(x)$ [T^{-1}], which is a measure of the hydraulic connectivity between the two domains (Fig. 1). This concept has been used extensively in studies concerned with the interactions of surface–subsurface flow and is also

Fig. 1. Schematic of the conductance concept (left) with an interface of thickness $\dot{m}$, which is represented by the conductance coefficient λ in theoretical models. The more general overland flow boundary is shown on the right.

known as the conductance concept with λ being the conductance coefficient [18,2].

Often the system of equations outlined above is solved iteratively. For example, one might iterate over q_e until some convergence criteria is fulfilled. However, since overland flow time scales may be much smaller than groundwater flow time scales, numerical instabilities often arise, necessitating adaptive time stepping and/or a fully integrated approach to solve the system of equations simultaneously (e.g., [32]).

This approach assumes the existence of a distinct interface between the surface and subsurface, which results in the definition of the proportionality constant, λ. For example, λ often depends upon the ratio of some interface permeability k' and the interface thickness m'. As mentioned previously, it is difficult to establish evidence of and values for such a proportionality constant from direct field observations [7,25]. Often a simplifying assumption of spatial uniformity in the hydraulic interface properties is applied, because of this lack of field data. In many cases, no in situ measurements are available and λ is used solely as a fitting parameter [4,15].

2.4. A general coupled surface–subsurface formulation

The previous section summarizes the current approach and points to the need for a more general formulation of the coupled surface–subsurface system. A formulation that directly couples the system of equations via the boundary condition at the ground surface is presented below. This formulation eliminates some of the problems associated with the definition of an interface conductance and possible numerical difficulties associated with the solution of the coupled system.

As shown in Fig. 1, the overland flow equations may be implemented into the Richards equation at the top boundary cell under saturated conditions. Using conditions of continuity of pressure ($\psi_s = \psi_p = \psi$) and flux ($q_{bc} = q_e$) at the ground surface (Fig. 1), Eq. (1) can be solved for q_e

$$q_e(x) = \frac{\partial\|\psi, 0\|}{\partial t} - \nabla \vec{v} \|\psi, 0\| - q_r(x) \quad (11)$$

and then substituted for q_{bc} in the boundary condition in Eq. (9):

$$-k(x)k_r\nabla(\psi - z) = \frac{\partial\|\psi, 0\|}{\partial t} - \nabla \vec{v} \|\psi, 0\| - q_r(x), \quad (12)$$

where $\|A, B\|$ indicates the greater of A and B. This formulation results in the surface water equations being represented as a boundary condition to the Richards Equation. The assumption of pressure continuity states that the pressures of the surface and subsurface domains are continuous (equal) right at the land surface. Thus, we are left with one computational node right at the land surface representing the surface–subsurface domain
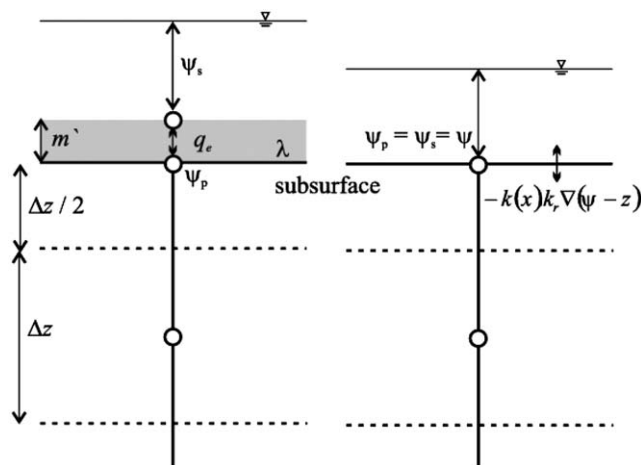
simultaneously via Eq. (12), which removes the conductance concept and the exchange flux q_e from the equations. This new boundary condition is head-dependent and accounts for the movement of the free surface of ponded water at the ground surface. In Eq. (12), if one assumes no lateral flow ($\nabla \vec{v}\, \psi = 0)$) and no recharge/precipitation ($q_r(x) = 0$) the infiltration/exfiltration rate $-k(x)k_r\nabla(\psi - z)$ equals the velocity $\frac{\partial \psi}{\partial t}$ of the free surface of ponded water, $-k(x)k_r\nabla(\psi - z) = \frac{\partial \psi}{\partial t}$. A similar formulation has been used by Neuman [31] and Moench [30] to account for the movement of the free water table of an unconfined aquifer.

Eq. (6) now reduces to

$$S_s S_w \frac{\partial \psi_p}{\partial t} + \phi \frac{\partial S_w}{\partial t} = \nabla \cdot [k(x)k_r(\psi)\nabla(\psi - z)] + q_s, \quad (13)$$

with q_e being accounted for in the new overland flow boundary condition (Eq. (12)), which intrinsically couples the surface and subsurface domains.

2.5. Discretization and numerical implementation

The discretization and numerical implementation of the variably saturated groundwater flow equation has been discussed in detail (e.g., [20]). The current formulation builds upon the works of Jones and Woodward [22] and only the details pertinent to the new overland flow boundary condition are presented here. Jones and Woodward employed an implicit backward Euler and cell-centered finite difference scheme for the discretizations in time and space, respectively. At the cell interfaces, the harmonic averages of the saturated hydraulic conductivities and a one-point upstream weighting of the relative permeabilities are used.

For the overland flow component, a standard upwind finite control volume scheme was used for the spatial discretization [33] and an implicit backward Euler scheme in time. The advantage of the spatial discretization methods applied in this study is that they are locally mass conservative. Discretization errors for the Richards equation have been analyzed extensively by Woodward and Dawson [46].

The solver implemented in the current study is described by Jones and Woodard [22] and is a Newton–Krylov solution method (e.g., [36]). Newton–Krylov methods are based on a Newton linearization of the nonlinear system. The Jacobian is then solved with an iterative Krylov method. An advantage of this method is that the Krylov solver only requires matrix–vector products not the solution of the matrix itself. Additionally, Jones and Woodward [23] preconditioned the linear system with an approximated Jacobian to improve convergence. In this study, the diagonal of the preconditioner matrix was modified to account for the overland flow boundary condition. This proved to be an efficient approximation of the Jacobian.

3. Numerical simulations, results and discussion

No analytical solution exists for the coupled surface–subsurface system of equations presented in Section 2. This makes model verification of the coupled system problematic. The approach taken here is to verify the overland flow simulator, validate the coupled model, and present a series of coupled simulation examples. The overland flow simulator was verified by comparing results to an analytical solution and other overland flow models and the coupled model was validated against a laboratory experiment. The modeling examples presented in this section focus on the two major processes of runoff production, that are, excess saturation and excess infiltration. The influence of spatially discrete subsurface heterogeneity (in form of a low-conductivity slab) on the hydrograph is studied. Additionally, we present the results from a simulation where the saturated hydraulic conductivity is represented as a space-random function using a small number of realizations. This study provides an example of the uncertainty in the simulated hydrograph due to uncertainty in subsurface heterogeneity. We conclude this section with a parallel scalability study of both the overland flow simulator and the fully coupled surface–subsurface flow model.

3.1. Model verification and validation

The numerical solution of the overland flow equations was verified by comparing to results published in Panday and Huyakorn [32] and to an analytical solution. The Panday and Huyakorn [32] results are for a two-dimensional tilted V-catchment (Fig. 2) for both, the gradient and critical depth outlet conditions. Additionally, Panday and Huyakorn [32] provided results from some commonly used hydrologic simulation models, such as HSPF [5] and HEC-1 [41], the results of which are also shown here (Fig. 3). The analytical solution used in the verification procedure describes a
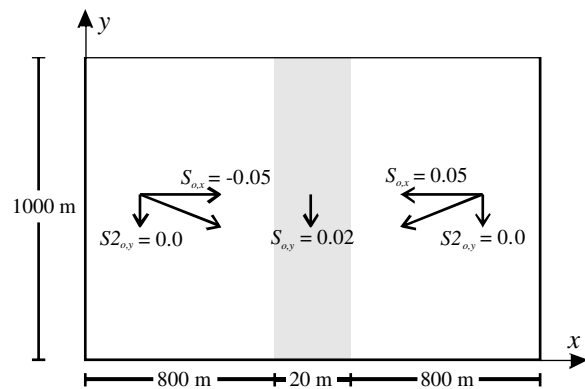
Fig. 2. Plan view (not to scale) of the problem setup of the tilted V-catchment after Panday and Huyakorn [32].
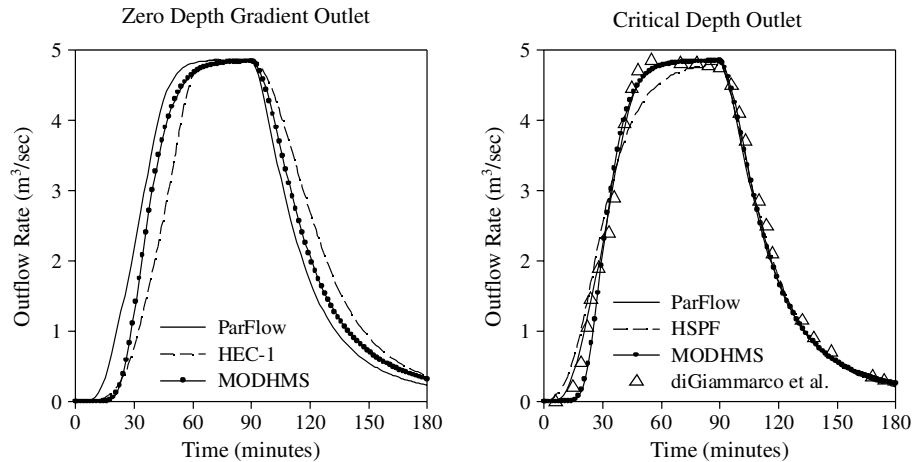
Fig. 3. Comparison of simulated hydrographs for the V-catchment problem for a number of hydrologic simulation models and ParFlow.

one-dimensional overland flow system. Note that analytical solutions only exist for the one-dimensional case. The coupled model was validated using results from a laboratory experiment by Abdul and Gillham [1].

3.1.1. The 2D V-catchment case

The problem setup for the tilted V-catchment after diGiammarco et al. [9] and Panday and Huyakorn [32] is shown in Fig. 2. We simulated a $1.62 \text{ km} \times 1 \text{ km}$ catchment slanted in the x- and y-direction with a centrally-located outlet at $800 \text{ m} \leqslant x \geqslant 820 \text{ m}$, $y = 0$. The slopes of the catchment are inclined inward routing flow into the center channel. The Manning's roughness coefficients are 1.74×10^{-7} and 1.74×10^{-6} (day/m$^{1/3}$) for the slopes and the channel, respectively. An equidistant discretization of 20 m ($\Delta x = \Delta y$) was used. As described in diGiammarco et al. [9], for 90 min the rainfall rate was 3×10^{-6} m/s with a subsequent 90 min recession period (total simulation time of 180 min). A constant time step of 100 s was used. To compare with the other model results in Fig. 3, simulations with both outlet types, gradient and critical depth, were performed. Note, results of the HEC-1, HSPF, MODHMS, and diGiammarco et al. [9] simulations stem from Panday and Huyakorn [32].

Fig. 3 shows that the ParFlow simulations for the critical depth and gradient outflow conditions are similar, because the kinematic wave approximation was used. The ParFlow simulations for the gradient outflow condition agree well with the results from MODHMS [32] and HEC-1. The differences in model simulations are mainly due to application of the kinematic wave approximation. However, the differences are relatively small, because the topographic slopes are fairly large, which results in overland flow that is dominated by the gravity force (or kinematic) term.

The differences become smaller in the case of the critical depth outflow condition, due mainly to higher outflow during earlier simulation times. This results

in a general decrease in the flow depth and less influence of the pressure force (or diffusive term) in the diffusive wave approximation used in e.g., MODHMS. The use of a constant time step in ParFlow that is more than an order of magnitude larger than the minimum time step of 5 s used in the MODHMS also contributes to differences at early simulation times. Overall the ParFlow model produces results that agree very well with other published results and lend confidence in the overland flow simulator in ParFlow. The fact that the solution method is based on the simpler kinematic wave approximation and does not explicitly distinguish between the channel and the land surface does not appear to affect the results significantly.

3.1.2. Comparison with 1D analytical solution

There exist few analytical solutions for overland flow problems. The one compared to here (e.g., [14]) is for a one-dimensional channel of constant slope and roughness. The parameters used in this comparison were obtained from Gottardi and Venuttelli [14] and Jaber and Mohtar [21] and are as follows: $S_{ox} = 0.0005$, $n = 2.3 \times 10^{-7}$ (day/m$^{1/3}$), and $q_r = 0.33$ (mm/min). Rainfall, q_r, was applied for 200 min followed by 100 min of recession ($q_r = 0$), which resulted in 300 min total simulation time. The time step size was constant at 180 s, as was the spatial discretization, $\Delta x = 80$ m. There were five cells in the x-direction ($nx = 5$) resulting in a total flow length of 400 m. The flow outlet was located at $x = 0$ and was simulated as a gradient outlet. For the remainder of the section this particular simulation is referred to as the base case.

Fig. 4 shows the comparison between the analytical and numerical solutions. Note that the differences at the time of concentration (t_c, when the outflow equals the rainfall rate) and at the end of the recession are due to the coarse spatial resolution used in the simulation. This figure also illustrates the improvement in
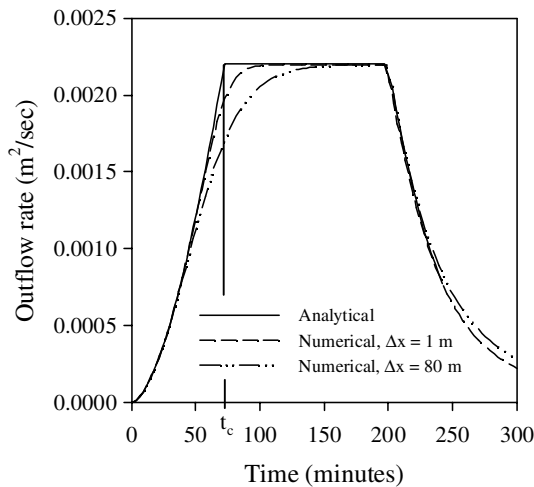
Fig. 4. Comparison between the numerical (symbols) and analytical solution (solid line) for two different Δx values.

reproducing the analytical solution, when the lateral discretization is decreased to $\Delta x = 1$ m (increasing the spatial resolution to $nx = 400$).

3.1.3. Validation of integrated surface–subsurface flow

Abdul and Gillham [1] reported the results of a laboratory experiment of overland flow generation. The experiments they performed consisted of a plexiglass tank 140 cm long, 8 cm wide, and 120 cm high. This tank was packed with medium-fine sand generating a sand body with a porosity of 0.34, a uniform slope of 12° and a Mannings surface roughness of 0.04 s/cm$^{1/3}$. An outlet was located at the right side of the box at a height of 74 cm. In one of their experiments, which was used in this study to validate the integrated surface/subsurface flow model, the initial water table was assigned at a height of 74 cm coinciding with the height of the outlet. A constant rainfall rate of 4.3 cm/h was applied uniformly for 20 min. At the outlet, the discharge was monitored continuously during the rainfall event and for a few minutes during the recession period after cessation of the rain.

Abdul and Gillham [1] also obtained the primary drying and wetting curves of the sand used in the experiments and the saturated hydraulic conductivity of 3.5 cm/s via permeameter tests. We visually fit the vanGenuchten model to both the drying and wetting curves to obtain α and n of Eqs. (7) and (8) (Fig. 5). The values are $\alpha_{\text{wetting}} = 0.024$ cm^{-1}, $n_{\text{wetting}} = 5$, $\alpha_{\text{drying}} = 0.015$ cm^{-1}, $n_{\text{drying}} = 8$. Note that it may be possible to arrive at better fits to the data using nonlinear regression techniques. For the purpose of testing the flow model, however, this visual fit proved sufficient to capture the general behavior of the saturation–pressure relationship.

In the flow model, the vertical and lateral discretization was 1 and 2 cm, respectively and a constant time
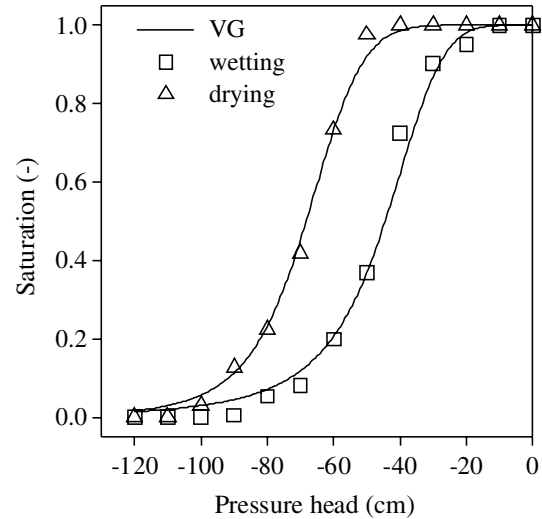

Fig. 5. Water content pressure head relationships: measured data (symbols) from Abdul and Gillham [1] and simulated data using the vanGenuchten model, VG ($\alpha_{\text{wetting}} = 0.024$ cm^{-1}, $n_{\text{wetting}} = 5$, $\alpha_{\text{drying}} = 0.015$ cm^{-1}, $n_{\text{drying}} = 8$).

step of 10 s was used. No-flow boundaries were assigned at the bottom and vertical sides of the domain allowing water to leave the domain only at the outlet.

Fig. 6 shows the measured data from Abdul and Gillham [1] and the simulation results using the parameters from the primary wetting curve. VanderKwaak [43] used the same experiment to verify the Integrated Hydrology Model (InHM). We included his simulation results here to additionally compare our results with a well-established flow model. Fig. 6 shows that the simulations results from ParFlow compare favorably with the results from InHM. Both models simulate earlier times of concentration and faster recession compared to the measured data, which can be explained with the
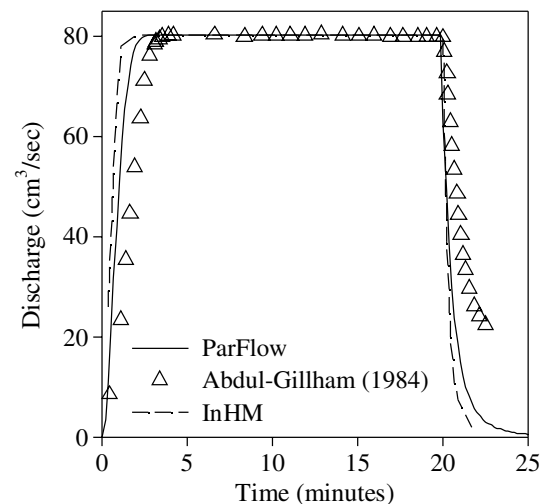

Fig. 6. Comparison of measured hydrograph by Abdul and Gillham [1] with simulation results using ParFlow and InHM [43].

lack of air phase compression in the applied models [1,43].

3.2. Integrated modeling examples

In this section, we present simulations that focus on the interaction of flow between the surface and subsurface. The runoff generating processes of excess saturation and infiltration are examined and compared to the 1D *base case*, which we defined in the comparison with the 1D analytical solution in Section 3.1. The influence of vertical spatial discretization and subsurface heterogeneity in the hydraulic conductivity on the resulting hydrograph is also investigated. In all cases, the gradient outlet condition is employed and a constant rainfall rate of $q_r = 0.33$ (mm/min) is applied for 200 min followed by 100 min of recession. Table 1 provides a summary of the different simulations.

3.2.1. Runoff production by excess saturation, $K_{sat} > q_r$

The process of excess saturation involves the complete saturation of the subsurface and the intersection of the land surface by the water table, where the exposed water table produces the runoff. To accomplish this, the hydraulic conductivity must be larger than the rainfall rate. We simulated two cases with a shallow water table initially located at a depth of 0.5 and 1.0 m below the ground surface. The vanGenuchten parameters and saturated hydraulic conductivity are as follows: $K_{sat} = 1.0$ m/day, $n = 2.0$, $\alpha = 1.0$, $\theta_{res} = 0.08$, $\theta_{sat} = 0.4$. The results of these two cases are shown in Fig. 7. Additionally, for each case, the sensitivity of runoff to the vertical discretization was explored. This was achieved by varying the constant vertical discretization from $\Delta z = 0.05$ to 0.2 m. Fig. 7 also shows the results from the base case for comparison. For excess saturation, Fig. 7 reveals, that the vertical discretization does not have a significant impact on the predicted outflow hydrograph. This can be seen by comparing the curves using different Δz values for a given water table depth. For the water table
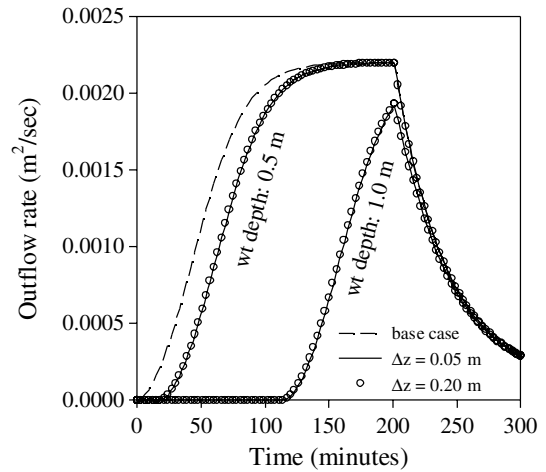

Fig. 7. Comparison of the base case with simulations using $q_r < K_{sat}$ and different vertical discretizations for water table depths of 0.5 and 1.0 m.

depth of 0.5 and 1 m, the times of ponding are some 19 and 117 min, respectively. For the 1 m initial water table depth, no steady state is reached and the outflow rate is always smaller than rainfall rate multiplied by the length of the channel.

3.2.2. Runoff production by excess infiltration, $K_{sat} < q_r$

The more complex process of excess infiltration involves the saturation of the surface and ensuing ponding of water, before the subsurface saturates completely. For excess infiltration to occur the saturated hydraulic conductivity of the surface must be smaller than the rainfall rate.

The results of these coupled simulations are shown in Fig. 8. The water table is initially located 1 m below the ground surface. The vanGenuchten parameters are the same as the previous set used in the excess saturation simulations. The saturated hydraulic conducti-
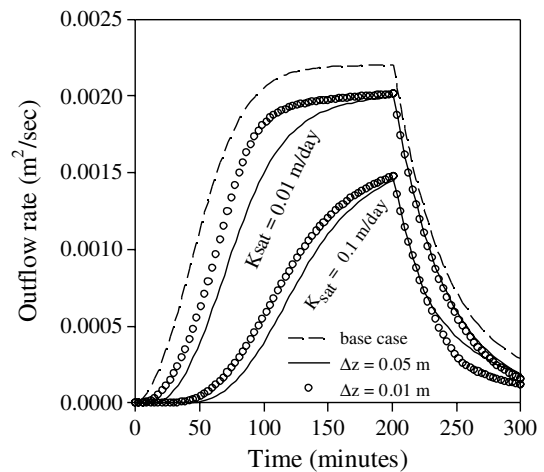
Table 1
Summary of the integrated modeling examples

Type	WT depth (m)	Δz (m)	K_{sat} (m/day)
Excess saturation, $K_{sat} > q_r$	1.0	0.2	1.0
		0.05	
	0.5	0.2	
		0.05	
Excess infiltration, $K_{sat} < q_r$	1.0	0.05	0.1
		0.01	
		0.05	0.01
		0.01	
Slab	1.0	0.05	Aquifer: 1.0, slab: 0.01
Monte Carlo	1.0	0.05	$K_g = 0.4752$, $\sigma[\ln(K_{sat})] = 3.0$

Fig. 8. Comparison of the base case with simulations using $q_r > K_{sat}$ and different vertical discretizations.

vity was varied from $K_{sat} = 0.1$ to 0.01 m/day and two different vertical discretizations were used ($\Delta z = 0.05$ and 0.01 m).

For cases where runoff is produced by excess infiltration, the vertical discretization has a significant impact on the ponding time (Fig. 8). This is because the top model layer holds a finite storage volume that must be saturated for ponding to occur (e.g., [10]). Thus, the solution becomes less accurate for large Δz values near the ground surface. A possible remedy to this problem is to make Δz very small at the land surface.

3.2.3. Subsurface heterogeneity in K_{sat}

A nonuniform spatial distribution of the hydraulic properties of the subsurface may have a significant impact on the observed hydrograph [47]. Therefore, it is important that an integrated flow model be able to account for subsurface heterogeneity. The ability of ParFlow to accommodate strongly heterogeneous parameter distributions has been demonstrated previously by Jones and Woodward [22], Tompson et al. [40] and Maxwell et al. [28] for subsurface flow problems. The following two examples will demonstrate the usefulness of this modeling approach in simulating interactions between surface water and groundwater under heterogeneous subsurface conditions.

The first example is a variation of the excess saturation case described above. The difference is the inclusion of a 100 m long, low-conductivity slab, $K_{sat} = 0.01$ m/day, located in the center of the domain extending from the land surface to a depth of 0.05 m. The initial water table was set to a depth of 1.0 m below the land surface and the vertical discretization was $\Delta z = 0.05$ m. Fig. 9 shows the resulting hydrograph and a comparison with the base case and the homogeneous excess saturation case.
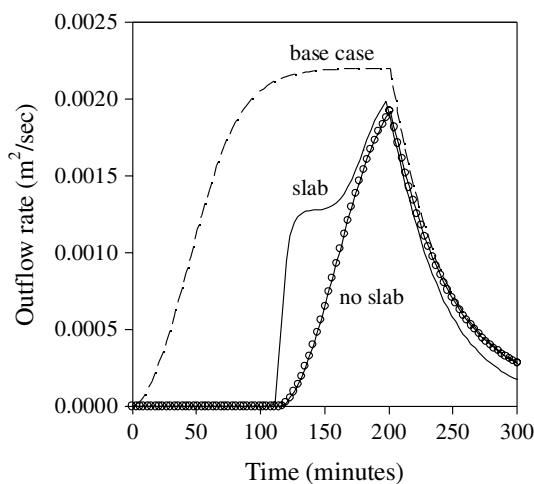

Fig. 9. Plot of the outflow hydrograph as a function of time with and without a low-conductivity slab located in the center of the domain along with the base case.
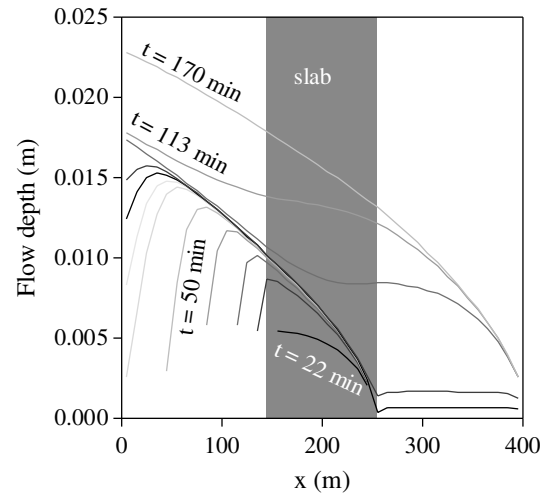

Fig. 10. Plot of simulated flow depth as a function of x (lateral profiles at the land surface) for different simulation times.

The simulated hydrograph is characterized by four distinct segments: two steep segments separated by a flat segment and a recession period after cessation of the rain (at $t = 200$ min), which makes up the fourth segment. Fig. 10 shows the temporal evolution of the flow depth distribution at the land surface, i.e., each curve represents a snapshot in time of the depth of ponded water at the land surface. Fig. 11 contains a time series of plots of the vertical relative saturation profiles of the domain starting from the initial conditions at $t = 0$. The step-like representation of the topography in ParFlow (e.g., Fig. 11) is a result of the lateral discretization, the topographic slope and the finite difference grid. Figs. 9–11 demonstrate the interactions and interdependence of excess infiltration and saturation processes in the presence of subsurface heterogeneity and are discussed in detail below.

The time series in Fig. 11 ($t = 39$ min) shows that ponding first occurs in the region of the low-K_{sat} slab, because of excess infiltration. This is also illustrated by the flow depth distribution in Fig. 10 at early times. The ponded water is routed over the slab and infiltrates downhill of the slab causing saturation of the subsurface, which subsequently reaches the ground surface. This process causes a saturation front to form and move from the slab toward the outlet (see plots for $t = 60$–102 min in Fig. 11).

Complete saturation of the subsurface results in the formation of a surface wave that reaches the outlet at about 110 min, which is reflected in the curves for $t < 110$ min in Fig. 10. The outflow rate increases sharply as the wave arrives at the outlet (first segment of the hydrograph shown in Fig. 9). At this time, the subsurface uphill from the slab is not fully saturated yet ($t = 111$ min). Shortly after the entire domain becomes saturated, the hydrograph flattens, and a
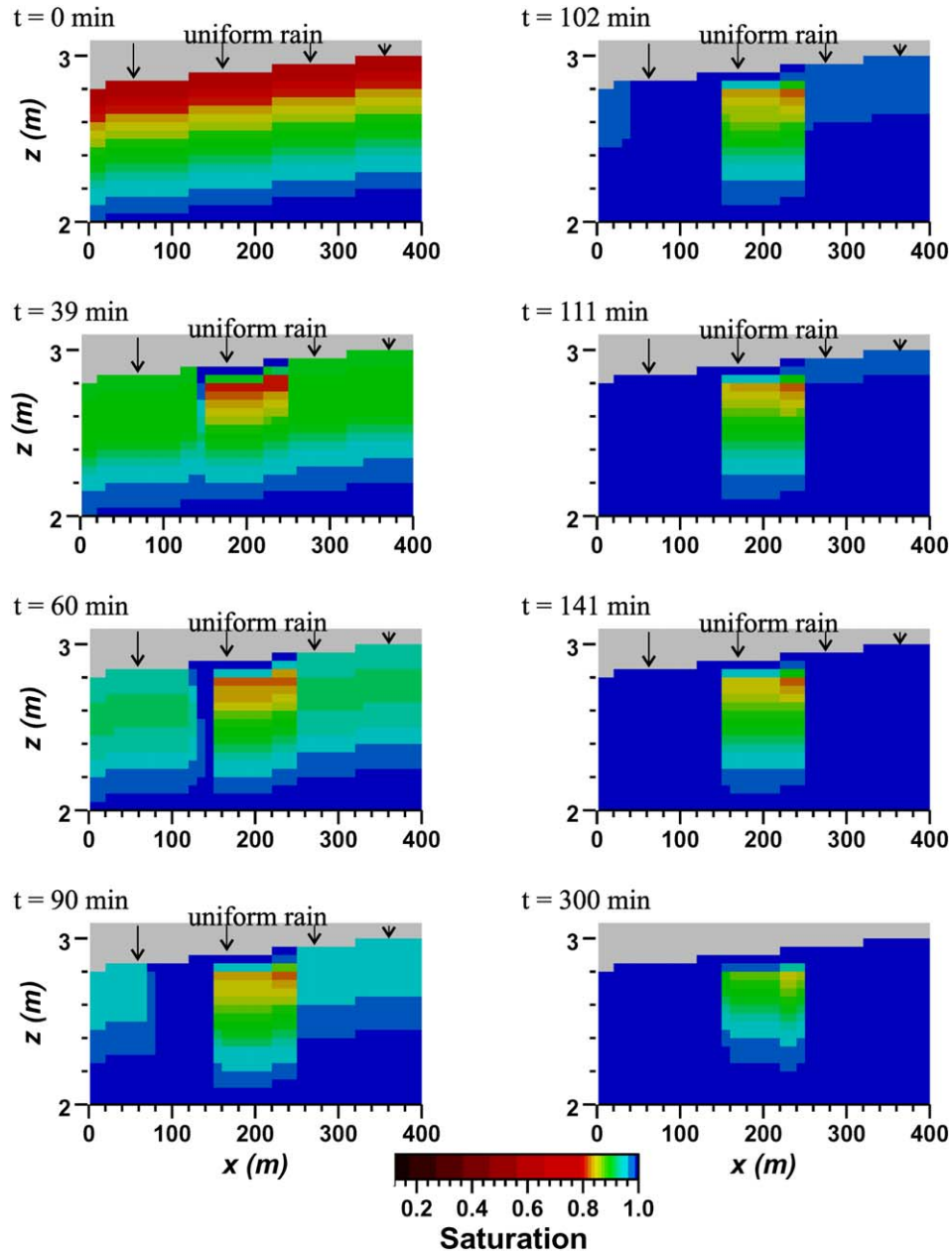
Fig. 11. Snapshots of vertical profiles of relative saturation at different simulation times (note the strong vertical exaggeration).

quasi-steady-state flow regime is reached for the period $135 < t < 150$ min (second segment). This is due to the stabilization of the flow depth profile along the slope downhill from the slab.

As soon as the subsurface is saturated completely uphill of the slab and, thus over the entire domain, a second wave is generated uphill of the slab that starts traveling toward the outlet (from $t = 117$ to 150 min). At 150 min, the outflow rate again increases sharply (third segment), when the second wave reaches the outlet ($t = 150$–200 min in Fig. 9). A second steady-state is not reached in this case, because there is not enough time for the flow depth profile to stabilize over the entire domain.

After cessation of the rain at $t = 200$ min, the outflow rate decreases monotonically during the recession period. The subsurface beneath the slab remains partially unsaturated over the entire simulation period, though lateral redistribution of soil moisture is clearly detectable from the plots in Fig. 11.

The second heterogeneous example consists of a set of simulations, where each simulation is based on a realization of random subsurface heterogeneity in K_{sat}. We used a hypothetical, correlated Gaussian random field to describe the distribution of the saturated hydraulic conductivity [39] with the following properties: geometric mean: $K_g = 0.4752$ m/day; standard deviation: $\sigma[\ln(k)] = 3.0$;

correlation lengths in horizontal and vertical direction, respectively: $\eta_h = 50.0$ m, $\eta_z = 1.0$ m. Different random seeds were used to generate four equally likely realizations of the K_{sat} distribution. Note that the geometric mean of the distribution is equal to the rainfall rate. This allows both runoff-generating processes (excess saturation and infiltration) to occur simultaneously in the simulations. The spatial distribution of these processes depends on the lateral K_{sat} distribution in the top layer of an individual realization. The initial water table depth was set at 1.0 m below the ground surface. The horizontal and vertical discretizations were set to 10 and 0.05 m, respectively, to capture the scale of the heterogeneity and the infiltration excess timing. For comparison, the model was also run for a case with effective parameters, a homogeneous saturated hydraulic conductivity, $K_{sat} = K_g = 0.4752$ m/day, referred to below as the *geometric mean simulation*.

Fig. 12 shows the hydrographs for four realizations of subsurface heterogeneity, the geometric mean simulation, and the base case. The spread in the curves for the different realizations is a measure of the uncertainty associated with the hydrograph due to uncertainty in the subsurface heterogeneity. Because all other parameters were kept constant and the rainfall rate was applied uniformly in space, this figure illustrates the direct impact of subsurface heterogeneity on the outflow rate. Comparing the geometric mean simulation with the different realizations, it can be seen that the geometric mean simulation provides generally smaller runoff rates at earlier times ($t < 150$ min), when the process of excess infiltration plays a dominant role in the production of runoff. For the duration $150 < t > 200$ min, the geometric mean simulation is bounded by the set of curves from the different realizations. During this time period excess saturation is the main runoff-generating process. The peak outflow rate, which occurs at $t = 200$ min, is larger
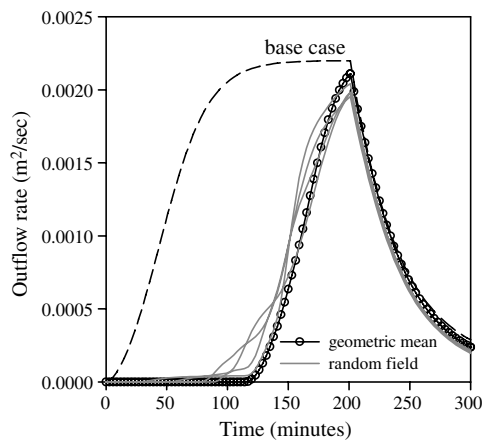
for the geometric mean simulation compared to the values from the four realizations.

Another process of runoff production, which can also occur due to aquifer heterogeneity, but can be seen as being different from the processes of excess infiltration and saturation, is the formation of a perched water table that intersects the ground surface. This process of runoff production is different from excess infiltration in that it forms saturated regions in the shallow subsurface not merely the ground surface itself. A perched water table and associated runoff can only be accounted for by explicitly incorporating aquifer heterogeneity into the flow model. This runoff-generating process contributed some of the early-time runoff in the different realizations. This resulted in larger runoff rates for some of the realizations of hydraulic conductivity when compared to the geometric mean simulation, which cannot account for a perched water table.

Fig. 13 shows the interdependence of the different runoff generating processes, such as a perched water table, due to the presence of aquifer heterogeneity for a single realization. The aquifer heterogeneity is indicated at the top, with K_{sat} varying over orders of magnitude. Inspection of the saturation profile at the

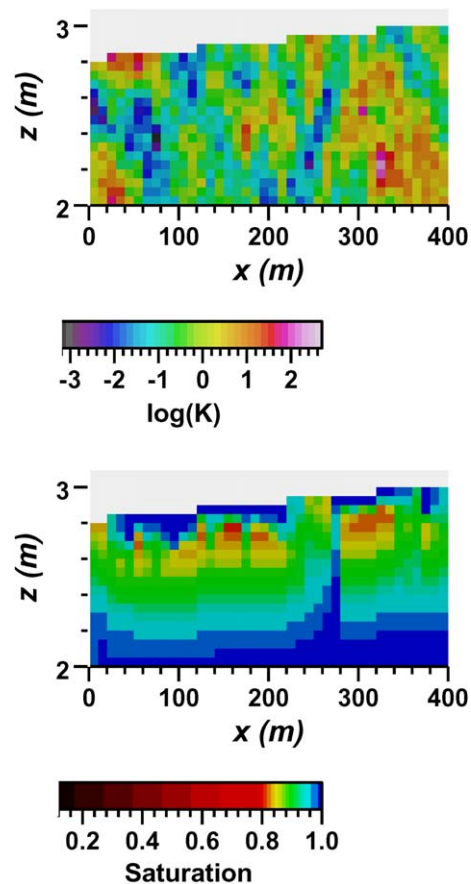Fig. 12. Results from the four Gaussian random field and geometric mean simulations. The base case is shown for comparison.

Fig. 13. Example of a K_{sat} distribution of a single realization (top) and the associated relative saturation profile after 45 min simulation time (bottom).

bottom of Fig. 13 reveals that there are regions of ponded water due to a region of low-conductivity heterogeneity right at the surface and in the shallow subsurface (e.g., perched water table at around $x \cong 180$ m). The profile also exhibits an interesting feature at $x \cong 280$, where a high conductivity path conveys the ponded water from the surface directly into the deeper aquifer, highlighting the importance of aquifer heterogeneity characterization and representation in coupled surface water groundwater systems. These features also indicate the importance of subsurface heterogeneity in coupled surface–subsurface problems concerned with mass transport.

3.2.4. Parallel scalability

A major advantage of ParFlow over other existing integrated hydrologic modeling tools is the infrastructure devised for massively parallel computer systems [3,22]. The overland flow simulator discussed here is designed to exploit this infrastructure and is, thus, massively parallel as well. A determining factor of parallel efficiency is the time the code spends on inter-processor communications (communication overhead) relative to the computation time. When the ratio between communication overhead and computation time is small, the parallel efficiency is large. Parallel efficiency of the overland flow simulator in ParFlow was studied by performing simulations of varying problem sizes and analyzing the respective run times. Following Jones and Woodard [22] the scaled efficiency, E, is defined as $E(n,p) = T(n,1)/T(pn,p)$, where T is the run time as a function of the problem size, n, which is distributed across a number of processors, p. For the case of a perfectly efficient parallel simulator, $E(n,p) = 1$, doubling the problem size and the number of processors will result in the same run time.

To test the parallel efficiency of the overland flow simulator, the *base case* from the comparison with the 1D analytical solution was used. In case of the integrated flow simulations, we used the excess infiltration case detailed in Section 3.2. In the latter, the unsaturated zone extended over five layers in the subsurface. The runs were performed on MCR at the Open Computing Facility of the Lawrence Livermore National Laboratory. MCR is a tightly coupled Linux cluster with a total of 2304 CPU's (Intel Xeon). In the scaling study, we used a maximum of 100 CPU's.

Fig. 14 shows E for two different model problems: overland flow only (surface) and for the case of excess infiltration produced runoff (surface/subsurface). The two different problems were run for a smaller number of model cells (nx,ny,nz) per processor $(20,20,1$ and $20,20,5)$ and for are larger number $(100,100,1$ and $100,100,5)$ to test the performance of the code for different communication overhead and computation time ratios.
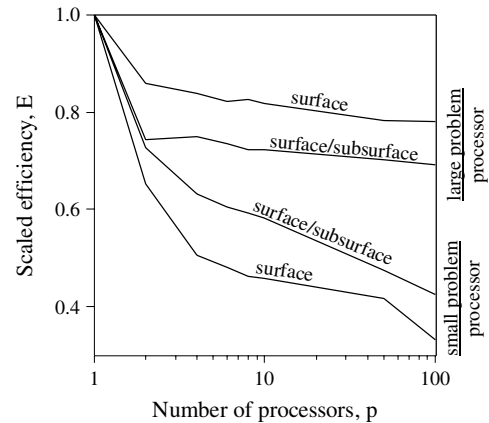

Fig. 14. Scaled parallel efficiency for simulations of surface flow only and surface/subsurface flow using small and large problem sizes per processor.

For the smaller problem size, the parallel efficiency of the excess infiltration case is significantly higher than for the overland flow only case. The scaled efficiency for the excess infiltration case declines steadily and approaches a value of around 0.4, whereas the scaled efficiency for the overland flow only case approaches a value of about 0.3 for 100 processors. This is due to relatively small computational times at individual processors for the overland flow only case and, thus, large communication overhead versus computation time ratios.

This trend, however, is reversed when the problem size at each processor is increased to $100,100,1$ and $100,100,5$. Fig. 14 shows a significant increase in the scaled efficiency for the overland flow only case, which now levels of at about 0.82. An increase, though smaller, is also observed in the saturation excess case, which now levels off at 0.72. This is due to larger increases in the computation time compared to the communication overhead and results in a smaller communication overhead versus computation time ratio demonstrating the parallel efficiency of ParFlow. Jones and Woodward [22] also performed a scalability study with ParFlow and arrived at 0.6 scaled efficiency for large problems and variably saturated flow. This compares well with the results of the presented scalability study in Fig. 14. In cases where ponding and overland flow occurs only in certain areas of the domain, load balancing may become an issue, i.e. processors with overland flow have considerable more computational work to do than other processors causing low parallel inefficiency.

4. Conclusions

A new formulation of coupled surface water–groundwater flow, which does not depend on a conductance-like relationship, has been described. This formulation forms the basis of an overland flow simulator based

on the kinematic wave approximation that has been implemented in the parallel, three-dimensional, variably saturated flow code ParFlow. The overland flow simulator takes the form of a free-surface upper boundary condition for the problem of variably saturated groundwater flow and is therefore fully integrated.

The overland flow simulator was verified using previously published data and an analytical solution. The fully coupled model was compared against a laboratory experiment and showed good agreement. Simulation examples were presented that focused on the two main processes of runoff production, excess saturation and infiltration. The effect of varying vertical discretization was also studied. Changes in the vertical discretization had a significant impact on the solution only in the case of excess infiltration, due to dependence of the time of ponding on the finite storage of the top layer.

We have shown that shallow subsurface heterogeneity may have a strong influence on the outflow rate and may cause a segmented hydrograph. A set of simulations where a heterogeneous subsurface was simulated as a correlated random field was used to demonstrate how uncertainty due to subsurface heterogeneity influences uncertainty in runoff predictions. A comparison with a homogeneous geometric mean simulation of the hydraulic conductivity showed that the geometric mean simulation may not account for excess infiltration and, thus, underestimates early parts of the hydrograph. Because the new, coupled formulation can explicitly account for subsurface heterogeneity, the production of runoff due to the formation of a perched water table can be simulated. This process of runoff production is often neglected by other hydrologic modeling tools, such as land surface models, and acts on a time scale between excess infiltration (short time scale) and excess saturation (long to very long time scale) depending on the depth of the water table from the ground surface.

A parallel efficiency study showed the excellent scalability of the overland flow simulator and the fully coupled surface–subsurface simulator for large problems. This makes this new, coupled model especially suitable for small and large watershed modeling, where the efficient use of large computational resources is vital.

Acknowledgements

References

[1] Abdul AS, Gillham RW. Laboratory studies of the effects of the capillary fringe on streamflow generation. Water Resour Res 1984;20(6):691–8.

[2] Anderson MP, Woessner WW. Applied groundwater modeling: simulation of flow and advective transport. San Diego: Academic Press; 1992. p. 281.

[3] Ashby SF, Falgout RD. A parallel multigrid preconditioned conjugate gradient algorithm for groundwater flow simulations. Nucl Sci Eng 1996;124(1):145–59.

[4] Bencala KE. Interactions of solutes and streambed sediments. 2. A dynamic analysis of coupled hydrologic and chemical processes that determine solute transport. Water Resour Res 1984;20(12): 1804–14.

[5] Hydrologic simulation program FORTRAN (HSPF): User's manual for release 10, EPA-600/R-93/174 Bicknell BR, Imhoff JL, Kittle JL, Donigian AS, Johanson RC. Athens, GA: US Environmental Protection Agency; 1993.

[6] Braunschweig F, Leitao PC, Fernandes L, Pina P, Neves RJJ. The object-oriented design of the integrated water modelling system MOHID. Proceedings of the XV international conference on computational methods in water resources (CMWR XV), Vol.2. Chapel Hill, NC, USA: Elsevier; 2004. p. 1079–90.

[7] Cardenas MBR, Zlontik VA. Three-dimensional model of modern channel bend deposits. Water Resour Res 2003;39(6):1141. doi:10.1029/2002WR001383.

[8] Applied Hydrology Chow VT, Maidment DR, Mays LW. Applied hydrology. Eliassen R, King PH, Linsley RK, editors. McGraw-Hill series in water resources and environmental engineering. McGraw-Hill, Inc.; 1988. p. 572.

[9] diGiammarco P, Todini E, Lamberti P. A conservative finite element approach to overland flow: control volume finite element formulation. J Hydrol 1996;175:267–91.

[10] Downer CW, Odgen FL. Appropriate vertical discretization of Richards' equation for two-dimensional watershed-scale modeling. Hydrol Process 2004;18:1–22.

[11] Fiedler FR, Ramirez JA. A numerical method for simulating discontinuous shallow flow over an infiltrating surface. Int J Numer Meth Fluids 2000;32:219–40.

[12] Forsyth PA, Wu YS, Pruess K. Robust numerical methods for saturated–unsaturated flow with dry conditions in heterogeneous media. Adv Water Resour 1995;18:25–38.

[13] Freeze RA, Harlan RL. Blue-print for a physically-based digitally simulated hydrologic response model. J Hydrol 1969;9:237–58.

[14] Gottardi G, Venutelli M. A control-volume finite element model for two-dimensional overland flow. Adv Water Resour 1993;16: 227–84.

[15] Govindaraju RS. Modeling overland flow contamination by chemicals mixed in shallow soil horizons under variable source area hydrology. Water Resour Res 1996;32(3):753–8.

[16] Govindaraju RS, Kavvas ML. Dynamics of moving boundary overland flows over infiltrating surfaces at hillslopes. Water Resour Res 1991;27(8):1885–98.

[17] Gunduz O, Aral MM. River networks and groundwater flow: a simultaneous solution of a coupled system. J Hydrol 2005;301: 216–34.

[18] Hantush MS. Wells near streams with semipervious beds. J Geophys Res 1965;70:2829–38.

[19] Huyakorn PS, Springer EP, Guvanasen V, Wadsworth TD. A three-dimensional finite element model for simulating water flow in variably saturated porous media. Water Resour Res 1986;22(12):1790–808.

[20] Huyakorn PS, Pinder GF. Computational methods in subsurface flow. New York: Academic Press; 1983.

[21] Jaber FH, Mohtar RH. Stability and accuracy of two-dimensional kinematic wave overland flow modeling. Adv Water Resour 2003;26:1189–98.

[22] Jones JE, Woodward CS. Newton–Krylov-multigrid solvers for large-scale, highly heterogeneous, variably saturated flow problems. Adv Water Resour 2001;24:763–74.

[23] Jones JE, Woodward CS. Preconditioning Newton–Krylov methods for variable saturated flow. In: Bentley LR, Sykes JF, Brebbia CA, Gray WG, Pinder GF, editors. Computational methods in water resources, Vol. 1. Rotterdam: Balkema; 2000. p. 101–6.

[24] Kirkland MR, Hills RG, Wierenga PJ. Algorithms for solving Richards' equation for nonuniform porous media. Water Resour Res 1992;28:2049–58.

[25] Kollet SJ, Zlontik VA. Stream depletion predictions using pumping test data from a heterogeneous stream-aquifer system (a case study from the Great Plains, USA). J Hydrol 2003;281: 96–114.

[26] Kutilek M, Nielson DR. Soil hydrology. GeoEcology. Cremlingen-Destedt, Germany: Catena Verlag; 1994. p. 370.

[27] LaBolle EM, Ahmed AA, Fogg GE. Review of integrated groundwater and surface water model (IGSM). Ground Water 2003;41(2):238–46.

[28] Maxwell RM, Welty C, Tompson AFB. Streamline-based simulation of virus transport resulting from long term artificial recharge in a heterogeneous aquifer. Adv Water Resour 2003;25(10):1075–96.

[29] Miller CT, Williams GA, Kelley CT, Tocci MD. Robust solution of Richards' equation for nonuniform porous media. Water Resour Res 1998;34:2599–610.

[30] Moench A. Flow to a well of finite diameter in a homogeneous, anisotropic water table aquifer. Water Resour Res 1997;33(6): 1397–407.

[31] Neuman SP. Theory of flow in unconfined aquifers considering delayed aquifer response. Water Resour Res 1972;8(4):1031–44.

[32] Panday S, Huyakorn PS. A fully coupled physically-based spatially-distributed model for evaluating surface/subsurface flow. Adv Water Resour 2004;27:361–82.

[33] Patankar SV. Numerical heat transfer and fluid flow. Minkowycz WJ, Sparrow EM, editors. Series in computational and physical processes in mechanics and thermal sciences. Taylor & Francis; 1980. p. 197.

[34] Putti M, Paniconi C. Time step and stability control for a coupled model of surface and subsurface flow. Proceedings of the XV International Conference on Computation Methods in Water Resources (CMWR XV), vol. 2. Chapel Hill, NC, USA: Elsevier; 2004. p. 1391–402.

[35] Richards LA. Capillary conduction of liquids through porous media. Physics 1931;1:318–33.

[36] Saad Y. Iterative methods for sparse linear systems. second ed. Philladelphia: SIAM; 2003.

[37] Taylor C, Al-Mashidani G, Davis JM. A finite element approach to watershed runoff. J Hydrol 1974;21:231–46.

[38] Therrien R, Sudicky EA. Three-dimensional analysis of variably-saturated flow and solute transport in discretely-fractured porous media. J Contam Hydrol 1996;23:1–44.

[39] Tompson AFB, Ababou R, Gelhar L. Implementation of the three-dimensional turning bands random field generator. Water Resour Res 1989;25(10):2227–43.

[40] Tompson AFB, Carle SF, Rosenberg ND, Maxwell RM. Analysis of groundwater migration from artificial recharge in a large urban aquifer: a simulation perspective. Water Resour Res 1999;35(10): 2981–98.

[41] USACE. HEC-1: Flood hydrograph package, user's manual, version 4.1, US Army Corps of Engineers, Hydrologic Engineering Center, Davis, CA, 1998.

[42] Van Genuchten MTh. A closed-form equation for predicting the hydraulic conductivity of unsaturated soils. Soil Sci Soc Am J 1980;44:892–8.

[43] VanderKwaak JE. Numerical simulation of flow and chemical transport in integrated surface–subsurface hydrologic systems. Ph.D. thesis, Department of Earth Science, University of Waterloo Center for Groundwater Research, University of Waterloo, Waterloo, Ont., Canada, 1999.

[44] VanderKwaak JE, Loague K. Hydrologic-response simulations for the R-5 catchment with a comprehensive physics-based model. Water Resour Res 2001;37(4):999–1013.

[45] Wallach R, Grigorin G, Rivlin(Byk) J. The errors in surface runoff prediction by neglecting the relationship between infiltration and overland flow depth. J Hydrol 1997;200:243–59.

[46] Woodward CS, Dawson CN. Analysis of expanded mixed finite element methods for a nonlinear parabolic equation modeling flow into variably saturated porous media. SIAM J Numer Anal 2000;37(3):701–24.

[47] Woolhiser DA, Smith RE, Giraldez JV. Effects of spatial variability of the saturated conductivity on Hortonian overland fow. Water Resour Res 1996;32(3):671–8.